Received: 10 March 2022 | Revised: 16 April 2022 | Accepted: 21 April 2022

DOI: 10.1002/ardp.202200121

FULL PAPER

ARCH PHARM DPhG
Archiv der Pharmazie

Thiazole-based SARS-CoV-2 protease (COV M^{pro}) inhibitors: Design, synthesis, enzyme inhibition, and molecular modeling simulations

Reham W. Elsayed | **Mohamed A. Sabry** | **Hussein I. El-Subbagh** | **Said M. Bayoumi** | **Selwan M. El-Sayed**

Department of Medicinal Chemistry, Faculty of Pharmacy, Mansoura University, Mansoura, Egypt

Correspondence
Hussein I. El-Subbagh and Selwan M. El-Sayed, Department of Medicinal Chemistry, Faculty of Pharmacy, Mansoura University, Mansoura 35516, Egypt.
Email: subbagh@yahoo.com and selwanmahmoud@hotmail.com

Abstract

As an attempt to contribute to the efforts of combating the pandemic virus severe acute respiratory syndrome coronavirus 2 (SARS-CoV-2) responsible for COVID-19, new analogs of the repurposed drug nitazoxanide which showed promising inhibitory efficacy on a viral protease enzyme were designed, synthesized and evaluated for their inhibitory activity on the main protease of the SARS-CoV-2 virus, using the COV2-3CL protease inhibition assay. The obtained results showed that the *N*-(substituted-thiazol-2-yl)cinnamamide analogs **19**, **20**, and **21** were the most active compounds with IC_{50} values of 22.61, 14.7, 21.99 μM, respectively, against the viral protease compared to the reference drugs, nitazoxanide, and lopinavir. Molecular modeling studies showed binding interactions of **19**, **20**, and **21** with hydrogen bonds to Gln189 and Glu166, arene–arene interaction between the thiazole moiety and His41, and other hydrophobic interactions between the ethene spacer moiety and Asn142. Moreover, an extra arene–arene interaction between substituted benzo[*d*]thiazole and His41 was observed regarding compounds **19** and **21**. Surface mapping and flexible alignment proved the structural similarity between the new drug candidates and nitazoxanide. Compliance of the new compounds to Lipinski's rule of five was investigated and absorption, distribution, metabolism, excretion, and toxicology data were predicted. The newly synthesized compounds are promising template ligands for further development and optimization.

KEYWORDS

COV Mpro inhibition, molecular modeling simulations, SARS-CoV-2, synthesis, thiazole-based derivatives

1 | INTRODUCTION

The global COVID-19 pandemic, induced by the virus severe acute respiratory syndrome coronavirus 2 (SARS-CoV-2), began to appear in December 2019 in Wuhan, China.[1] COVID-19 is characterized by respiratory pneumonia that ranges from mild pulmonary obstruction to severe respiratory depression. Also, it can affect the gastrointestinal tract and central nervous system and may lead to death.[2–4] According to the announced World Health Organization situational reports, many SARS-CoV-2 infection cases were globally confirmed,

including numerous deaths, and great attention was paid by medicinal chemists to find a medication for treatment.[5] SARS-CoV-2 belongs to a large virus family called coronaviruses (Coronaviridae) that share single-stranded RNA surrounded by a membrane envelope supplied with spikes that give them the characteristic crown-like appearance.[6] This family was divided into five major classes: alpha, beta, gamma, delta, and omicron. It has 30,000 nucleotides that encode four structural proteins, namely, spike (S), envelope (E), membrane (M), nucleocapsid (N), and others, which are nonstructural proteins comprehending papiane-like protease (PL^{pro}), RNA dependent polymerase (RdRp), coronavirus like protease (COV M^{pro}).[7–9] Once SARS-CoV-2 enters the host cells, it injects its RNA and starts to synthesize its own nonfunctional polyproteins using the host cell genome. These polyproteins are then cleaved into functional proteins through viral COV M^{pro} and PL^{pro}, so COV M^{pro} has an essential role in viral replication cycle and could be a critical target for designing anticovid drugs.[10] The main protease COV M^{pro} inhibitor, an isoxazole containing peptide, **N3** was successfully crystallized and submitted to the Protein Data Bank.[11] This facilitates its usage for in silico drug design studies.

Nitazoxanide is an approved antiparasitic drug that showed promising inhibitory action on the SARS-CoV-2 protease enzyme, so could be used as starting point for developing a series of new compounds sharing its main structural features.[12] Some modifications were introduced to its structure hoping to improve its inhibitory efficacy on viral protease. In the present investigation, keeping in mind the structural features of **N3**, designed modifications to nitazoxanide structure were performed to generate a series of thiazole-based analogs (**A**–**C**, Figure 1). The acetylsalicylic acid amide segment of nitazoxanide was replaced by cinnamamide (with an ethene moiety as a spacer); and the 2-nitro-thiazole segment was replaced with 4-(bromo or methyl)-phenyl-thiazole, 5-(bromo or methyl)thiazole, substituted benzo[*d*]thiazole, and ethyl thiazole-4-carboxylate. These chemical function alterations and electronic modifications were proposed to investigate the effect of these chemical changes on activity and to explore their inhibitory efficacy on COV M^{pro} using 3CL protease inhibition assay and molecular modeling simulations.

2 | RESULTS AND DISCUSSION

2.1 | Chemistry

The synthesis of the designed compounds (**A**–**C**; Figure 1) was attained as shown in Scheme 1. Different substituted 2-aminothiazole derivatives **1**–**3**, **11**, **12**, **17**, and **18** were allowed to react with cinnamoyl chloride (**4**) in pyridine to produce *N*-(thiazol-2-yl)-cinnamamide derivatives **5**–**7**, **13**, **14**, **19**, and **20** using experimental conditions previously described.[13,14] Methylation of the (NH) of the amide groups in those intermediate cinnamamide derivatives was achieved via stirring with methyl iodide in chloroform in presence of potassium carbonate to afford the *N*-methyl-*N*-(thiazol-2-yl)-cinnamamide derivatives **8**–**10**, **15**, **16**, **21**, and **22**. ^{1}H NMR spectra of the target compounds showed two characteristic olefinic absorptions appeared as a doublet at δ 6.2–6.5 and 7.7–7.9 ppm with coupling constant J = 15.6–15.8 Hz that confirmed *E* configuration. ^{1}H NMR spectra of the final compounds showed singlet absorptions for CH_3 at δ 3.9 ppm and their corresponding carbons appeared at δ 34.5–36.5 ppm in the ^{13}C spectra. The newly synthesized compounds

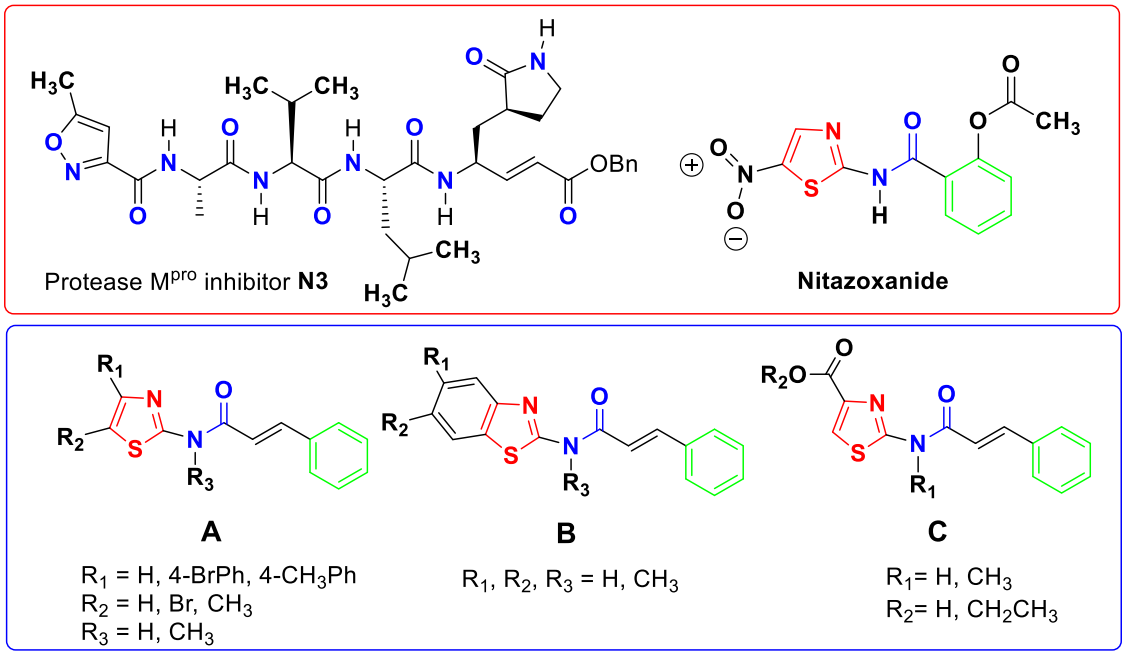

FIGURE 1 The protease (COV M^{pro}) inhibitor **N3** and a list of structures of the proposed thiazole-based analogs (**A**–**C**) as SARS-CoV-2 protease (COV M^{pro}) inhibitors.

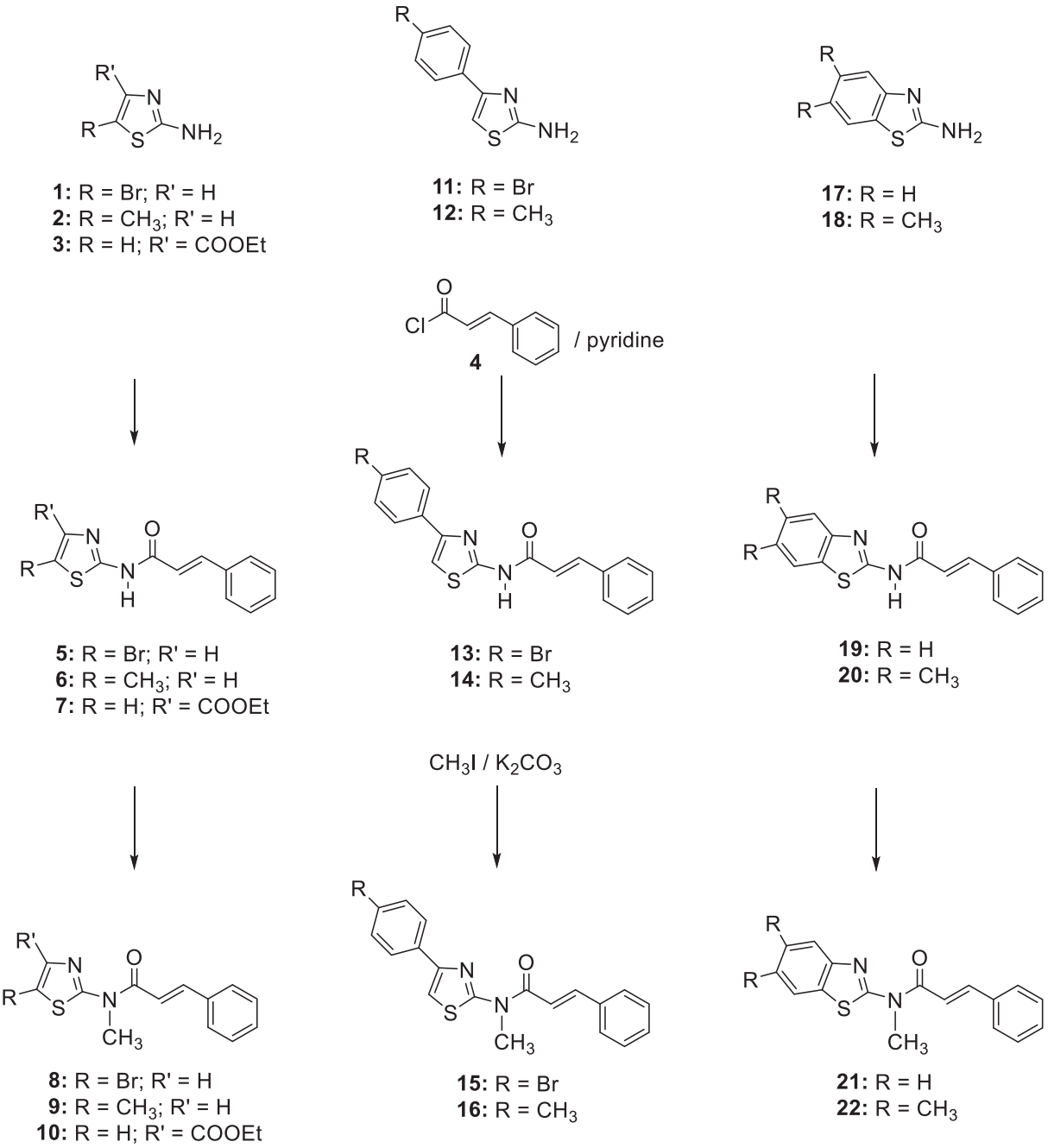

SCHEME 1 Synthesis of the target compounds **8**–**10**, **15**, **16**, **21**, and **22**.

were further elucidated by the mean of mass spectra and elemental analyses.

2.2 | COV2-3CL protease inhibition assay

The newly synthesized compounds **5**–**10**, **13**–**16**, **19**–**22** were subjected to COV2-3CL protease inhibition assay adopting the reported procedure.[15,16] Lopinavir was used as a standard drug with an IC_{50} value of 2.068 μM (Table 1). In general, the obtained results revealed that the synthesized compounds expressed modest activity (14.7–54.9 μM) compared to the reference compound. Compounds **19**, **20**, and **21** were the most active COV2-3CL protease inhibitors in this study with IC_{50} values of 22.61, 14.7, and 21.99 μM, respectively. Also, compounds **7** and **22** showed moderate activity with IC_{50} values of 30.72 and 34.14 μM, respectively. Moreover, compound **9** with IC_{50} (54.9 μM) showed weak activity while other compounds were inactive.

These results suggested that the replacement of the aminothiazole ring with a benzothiazole fused ring system that afforded compounds **19**, **20**, **21**, and **22** produced strong antiviral activity where their IC_{50} values were 22.61, 14.7, 21.99, and 34.14 μM,

TABLE 1 Results of COV2-3CL protease inhibition (IC_{50}, μM) of the target compounds **5–10**, **13–16**, and **19–22**.

Compound	R	R′	% Inhibition (ng/ml) 0.1	1	10	100	COV2-3CL protease (M^{pro}) IC_{50} (μM)[a]
5	Br	H	0.949	5.079	13.49	61.45	116.70 ± 6.17
6	CH_3	H	1.529	3.879	14.61	58.94	142.60 ± 7.53
7	H	COOEt	5.079	13.51	31.45	68.15	30.72 ± 1.62
8	Br	H	0.209	3.139	7.979	55.14	293.80 ± 15.5
9	CH_3	H	2.369	8.719	23.15	65.18	54.90 ± 2.9.0
10	H	COOEt	1.289	3.769	11.47	50.77	421.50 ± 22.30
13	Br	–	2.459	7.239	21.08	58.44	105.60 ± 5.58
14	CH_3	–	0.919	4.839	13.46	51.64	322.20 ± 17.0
15	Br	–	0.539	4.969	17.54	61.66	93.56 ± 4.95
16	CH_3	–	1.569	7.929	20.49	57.62	113.50 ± 6.0
19	H	–	5.359	16.4	33.09	71.57	22.61 ± 1.20
20	CH_3	–	5.379	15.37	38.61	77.05	14.70 ± 0.78
21	H	–	3.189	8.969	33.92	73.98	21.99 ± 1.16
22	CH_3	–	2.509	7.469	27.17	70.46	34.14 ± 1.80
Lopinavir	–	–	11.93	27.66	50.64	78.58	2.068 ± 0.11
Nitazoxanide	–	–	–	–	–	–	2.120

[a]IC_{50} values are the mean ± SD of three separate experiments.

respectively. While other structural modifications including 4-phenyl thiazole and substituted thiazole scaffolds were of no value regarding the antiviral activity where they afforded almost inactive compounds. This illustrated that the benzothiazole scaffold favored the activity rather than a thiazole or substituted thiazole ring system.

2.3 | Molecular modeling simulations

Molecular modeling methods are commonly used for efficient investigation of the structure, surface properties, and thermodynamics of chemical and biological systems.[17] Docking is an essential branch of molecular modeling that is used to simulate the chemical binding between different drug candidates and biological targets to predict their binding scores and binding interactions which refer to their affinity to the target and, hence, their biological activity.[18]

2.3.1 | Molecular docking

The binding interactions of the investigated compounds **5–10**, **13–16**, and **19–22** with the active site of main protease and their conformational analyses were performed using the Molecular Operating Environment (MOE) program. The results were compared to nitazoxanide, its active metabolite (tizoxanide), and lopinavir[12,19] as reference Covid-19 protease inhibitors. In this study, molecular docking was performed utilizing the crystal structure of the SARS-CoV-2 main protease in a complex with **N3** as an inhibitor (PDB ID: 6LU7). The docking process was validated through redocking of **N3** which is an inhibitor of SARS-CoV-2 M^{pro} and the root mean square deviation (RMSD) value was 1.5904.[11] The docking scores and types of binding interactions of the tested compounds and the reference drugs were illustrated in Table 2.

The docking results illustrated that the interaction of nitazoxanide to the SARS-CoV-2 protease (Figure 2a) includes hydrogen bonding between the central aromatic amide, peripheral ester, and His164, Glu166, respectively; besides an arene–arene interaction between the thiazole moiety and His41. Other strong hydrophobic interactions with Gln189, Met49, and Met165 were also noticed. Also, the interaction of lopinavir (Figure 2b) to SARS-CoV-2 protease includes H-bonding between central hydroxyl and Gln189, an arene–arene interaction between phenoxy moiety and His41, and other strong hydrophobic interactions with Asn142, Met165, Met49, Glu166, Leu141, and Pro168. Also, tizoxanide showed a hydrogen bond with Gln189 and arene–arene interaction with His41. Moreover, strong hydrophobic interactions with Glu166, Asn142, Cys145, Asp187, Leu141, Met49, and Met165 were observed. Regarding the binding interactions of the newly synthesized compounds, it could be observed that the new structural modifications that were introduced to the structure of nitazoxanide were valuable in binding to the COV M^{pro}. Where it was revealed that all of the binding interactions between the reference drug with the binding site were retained and some new additional bonding interactions. The introduction of the ethene spacer group led to a new strong hydrophobic interaction with Asn142 as could be noticed in the interaction of compound **19**

TABLE 2 The docking scores[a] and type of binding interactions of the designed compounds (**5–22**) with the SARS-CoV-2 main protease enzyme and the reference compounds nitazoxanide, tizoxanide, and lopinavir and N3.

Compounds	Binding energy (kcal/mol)	Type of binding interactions
5	−7.1	• Strong hydrophobic interaction with Glu166, Met49, Met165, Gln189, and Asn142.
6	−6.9	• Strong hydrophobic interaction with Glu166, Asn142, Gln189, and Met165.
7	−7.2	• H-bond with Gly143. • Strong hydrophobic interaction with Gln189, Met165, Glu166, Met49, Thr190, Thr26, Cys165, and His41.
8	−6.6	• Strong hydrophobic interaction with Gln189, Met165, Glu166, and Pro168.
9	−7.7	• Strong hydrophobic interaction with Gln189, Glu166, Asn142, Met49, and Met165.
10	−6.8	• Strong hydrophobic interaction with Glu166, Gln189, Asn142, and Met165.
13	−6.9	• Strong hydrophobic interaction with Glu166, Gln189, and Thr190.
14	−7.0	• Strong hydrophobic interaction with Glu166, Asn142, Thr24, Thr25, and Cys145.
15	−6.5	• Strong hydrophobic interaction with Glu166, Gln189, Asn142, Leu141, and Thr190.
16	−6.3	• Strong hydrophobic interaction with Glu166, Gln189, Cys145, Thr26, Gly143, and Met165.
19	−8.1	• Two arene–arene interactions with His41. • Strong hydrophobic interaction with Glu166, Asn142, Gln189, Met49, and Met165.
20	−8.5	• Two H-bond with Gln189 and Glu166. • Strong hydrophobic interaction with Met49, Met165, Cys145, Thr190, and His41.
21	−8.5	• Two arene–arene interactions with His41. • Strong hydrophobic interaction with Gln189, Glu166, Asn142, Asp187, Cys145, Leu141, Phe140, Met49, and Met165.
22	−7.9	• Arene–arene interaction with His41. • Strong hydrophobic interaction with Asn142, Met165, Met49, Glu166, Gln189, and Thr190.
Lopinavir	−12.1	• H-bonds with Gln189. • Arene–arene interaction with His41. • Strong hydrophobic interaction with Asn142, Met165, Met49, Glu166, Leu141, and Pro168.
Nitazoxanide[b]	−9.3	• Two H-bonds with His164 and Glu166. • Arene–arene interaction with His41. • Strong hydrophobic interaction with Gln189, Met49, and Met165.
Tizoxanide	−10.0	• H-bonds with Gln189. • Arene–arene interaction with His41. • Strong hydrophobic interaction with Glu166, Asn142, Cys145, Asp187, Leu141, Met49, and Met165.
N3 inhibitor[c]	−11.9	• H-bond with Glu166. • Strong hydrophobic interaction with Asn142, Pro168, Gln189, Met49, and Met165.

Abbreviation: MOE, Molecular Operating Environment; SARS-CoV-2, severe acute respiratory syndrome coronavirus 2.

[a]Docking was performed using MOE 2009.10 towards the active site of the SARS-CoV-2 main protease (PDB ID: 6LU7) (RMS gradient of 0.01 kcal/Å mol).

[b]Nitazoxanide, tizoxanide, and lopinavir were used as positive controls.

[c]N3 inhibitor is an inhibitor of the SARS-CoV-2 main protease.

(Figure 2c). In addition, introduction of substituted benzo[*d*]thiazole moiety caused an extra arene–arene interaction with His41 as illustrated in compounds **19** and **21** (Figure 2c,e). Furthermore, *N*-methylation of the cinnamamide moiety introduced additional hydrophobic interaction with Met49 and Asn142 as could be seen in compounds **21**.

Regarding compound **20** (Figure 2d), although it showed no arene–arene interactions, it showed instead two hydrogen bonds between the (C=O), (NH) of the cinnamamide moiety and Glu166 and Gln189, respectively. These two hydrogen bonds with these two amino acids Glu166 and Gln189 could be seen in the two reference drugs nitazoxanide and lopinavir, respectively. In addition, strong hydrophobic interactions were observed with many amino acids in the binding pocket namely, Met49, Met165, Cys145, Thr190, and His41.

N3 binds to the target binding site in an almost similar way to that of nitazoxanide. The designed compounds (Table 2) also bind to

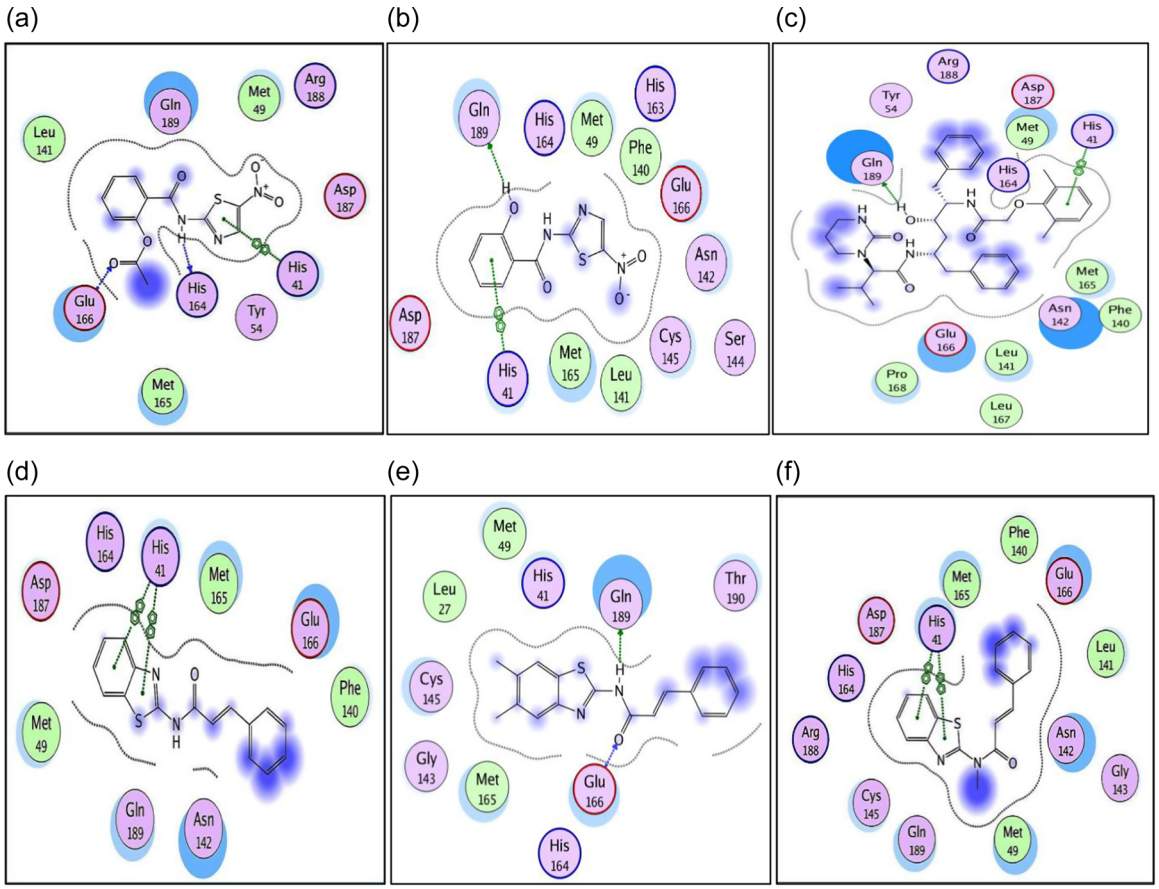

FIGURE 2 Two-dimensional binding mode and residues involved in the recognition of (a) nitazoxanide, (b) tizoxanide, (c) lopinavir, and the most promising designed compounds (d) **19**, (e) **20**, and (f) **21** docked and minimized in the SARS-CoV-2 main protease binding pocket. SARS-CoV-2, severe acute respiratory syndrome coronavirus 2.

SARS-CoV-2 protease active site amino acid residues by various binding interactions in a similar manner to that of the reference drug, in addition to binding through arene–arene interaction with His41.

Three-dimensional visualization of the docking results was shown in Figure 3 to simulate the most promising synthesized compounds **19**, **20**, and **21** binding to Covid-19 protease active pocket. Their results were compared to the reference drugs. These results showed that compounds **19**, **20**, and **21** have comparable good binding scores and promising binding affinities to the SARS-COV-2 viral protease pocket. Other modeling studies were performed to make sure that the studied compounds could be promising candidate drugs for Covid-19 treatment.

2.3.2 | Conformational analysis

To get a better insight into the molecular structure behavior of the most promising synthesized compounds **19**, **20**, and **21** in comparison to the reference SARS-CoV-2 protease inhibitor drug nitazoxanide, tizoxanide, and lopinavir, conformational analysis was performed using MMFF94 force-field[20] (with RMS gradient of 0.01 kcal/Å mol) implemented in MOE 2009.10.13 (Figure 4).

2.3.3 | Three-dimensional ligand-based alignment in SARS-CoV-2 protease pocket

Alignment of the docked ligands inside the SARS-CoV-2 protease binding pocket was performed and the binding pocket surface mapping showed that the most promising compounds **19**, **20**, and **21** occupied and filled the whole space of the binding pocket in a comparable manner to that of the reference drugs (Figure 5).

2.3.4 | Flexible alignment

Flexible alignment is a computational procedure used for flexibly aligning small molecules and computes a number of alignments. Three-dimensional alignment of candidate ligands can be used to conclude structural requirements for certain biological activity.[21] The good flexible alignment features used are derived from several points, such as the strain energy of each molecule is small, molecules have a similar shape and log *p* values, and that aromatic atoms, hydrophilic areas, and hydrophobic areas overlap. Figure 6 showed that nitazoxanide, tizoxanide, lopinavir, and the most promising compounds **19**, **20**, and **21** were perfectly aligned especially at the

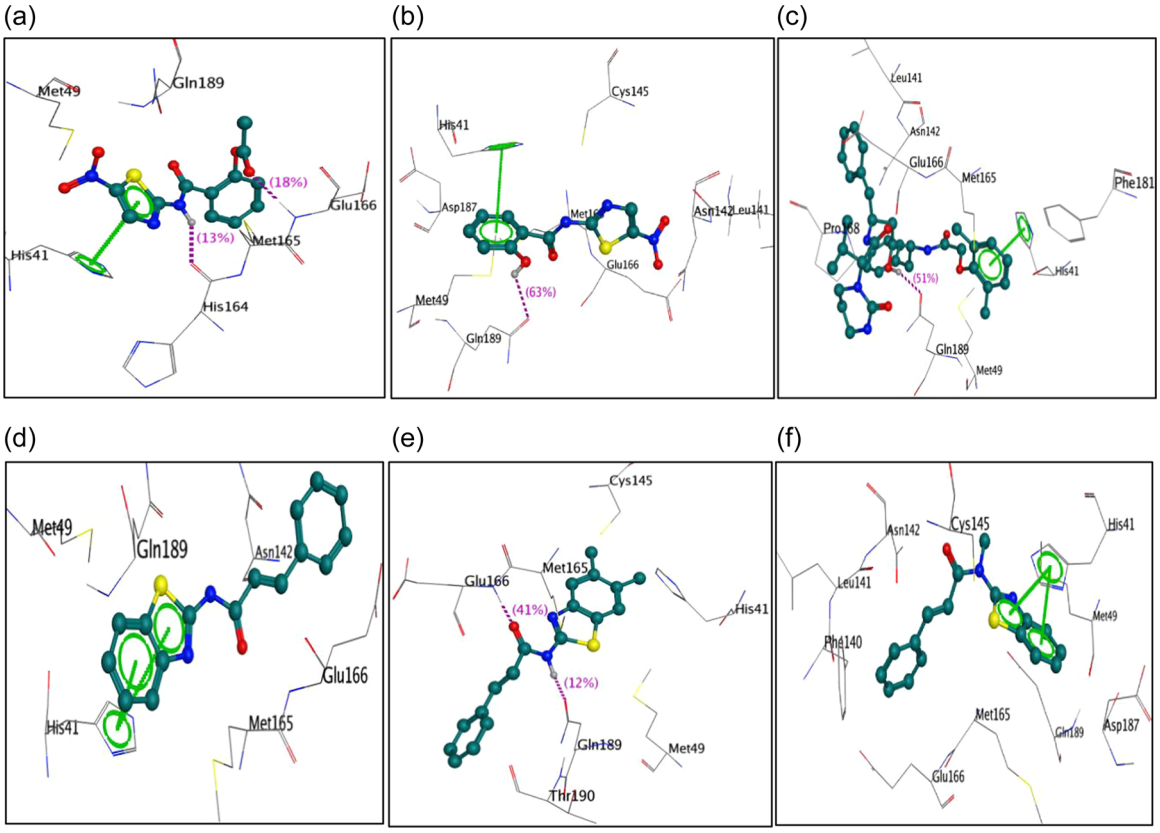

FIGURE 3 Three-dimensional binding mode and residues involved in the recognition of (a) nitazoxanide, (b) tizoxanide, (c) lopinavir, and the most promising designed compounds (d) **19**, (e) **20**, and (f) **21** docked and minimized in the SARS-CoV-2 main protease binding pocket. SARS-CoV-2, severe acute respiratory syndrome coronavirus 2.

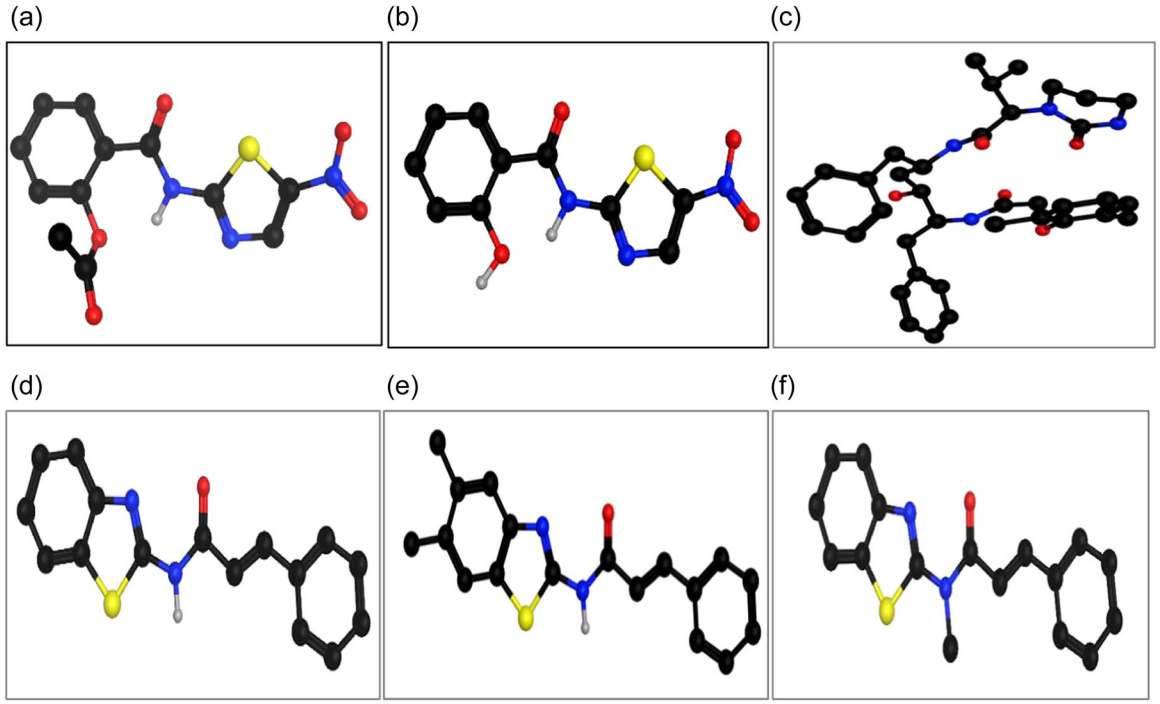

FIGURE 4 The lowest energy conformer of (a) nitazoxanide, (b) tizoxanide, (c) lopinavir, and the most promising compounds (d) **19**, (e) **20**, and (f) **21** in the ball and stick mode.

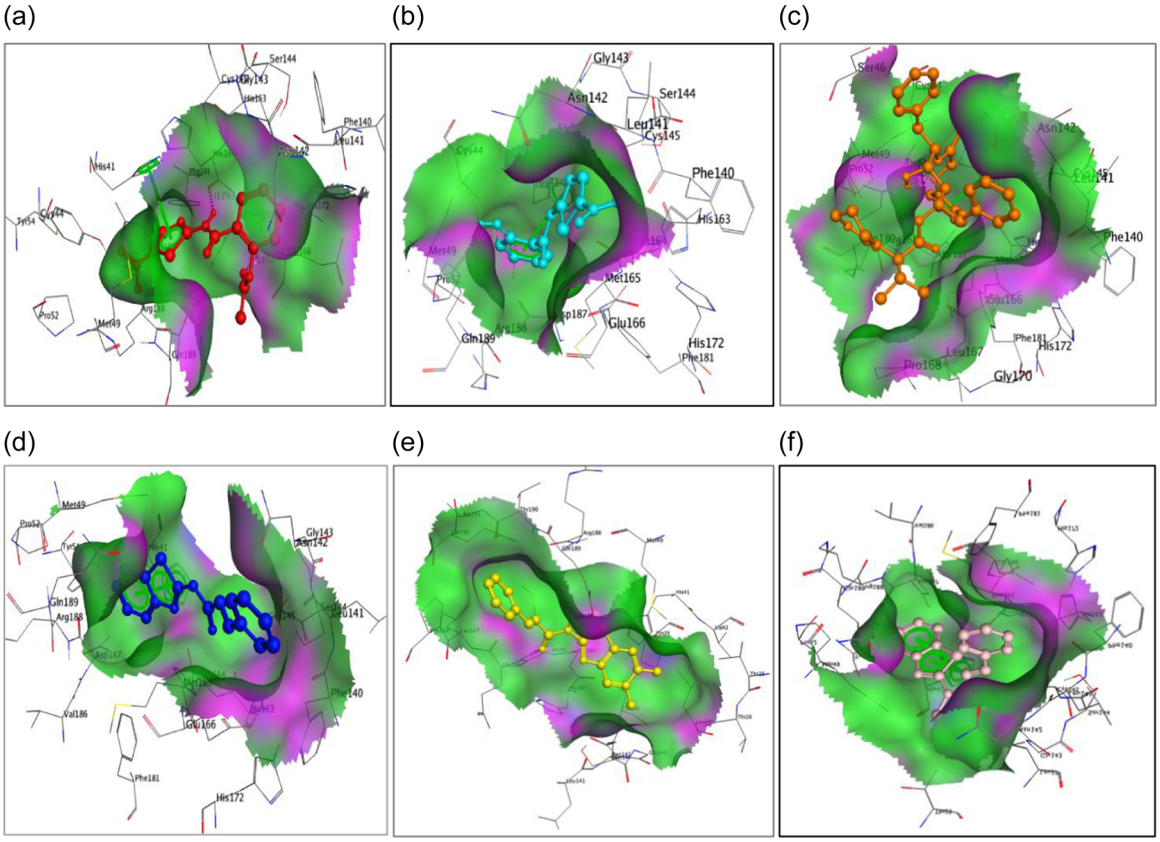

FIGURE 5 The aligned conformations of (a) nitazoxanide (ball and stick, red), (b) tizoxanide (ball and stick, cyan), (c) lopinavir (ball and stick, orange), and the most promising compounds (d) **19** (ball and stick, blue), (e) **20** (ball and stick, yellow), (f) **21** (ball and stick, pink) occupying the SARS-CoV-2 main protease binding pocket. SARS-CoV-2, severe acute respiratory syndrome coronavirus 2.

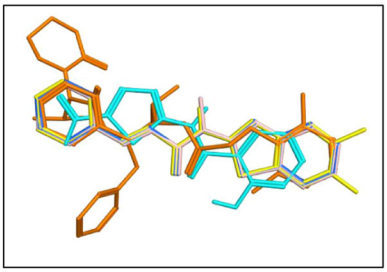

FIGURE 6 Flexible alignment of nitazoxanide (red), tizoxanide (cyan), lopinavir (orange), and the most promising compounds **19** (blue), **20** (yellow), and **21** (pink).

thiazole moiety. This explains the resemblance of the mode of binding between reference drugs and synthesized compounds.

2.3.5 | Surface mapping

Surface mapping is a molecular modeling tool that is used to visualize various physicochemical properties of the molecules on their atoms' surface. This method proves the importance of the relative distance and orientation between the essential binding groups.[22] Active lone pair (LP) surface mapping comparison of the most promising compounds **19**, **20**, **21** and the reference drugs nitazoxanide, tizoxanide, and lopinavir was performed to detect their surface properties and investigate the similarity in the position of hydrophilic and hydrophobic sites that bind to the active sites in SARS-CoV-2 protease pocket (Figure 7). Figure 8 shows another electrostatics surface mapping that is used to visualize the similarity of the surface charges of the designed compounds and their resemblance to the reference drugs. As noticed in Figures 7 and 8, it is clear that there is a large similarity between nitazoxanide, lopinavir, and the most promising synthesized compounds **19**, **20**, and **21** in having central neutral lipophilic regions and peripheral charged hydrophilic sites.

2.4 | Lipinski's rule of five

Lipinski's rule of five is a general guideline that is used to predict the drug-likeness and oral bioavailability by investigating the physico-chemical properties that might make a pharmacologically active compound an orally active agent in humans.[23] This rule is used in step-wise lead optimization of a pharmacologically active lead structure to enhance activity and selectivity, as well as drug-likeness as reported by Lipinski's rule.[24] Lipinski's rule states that any drug should not exceed one violation of certain criteria to be

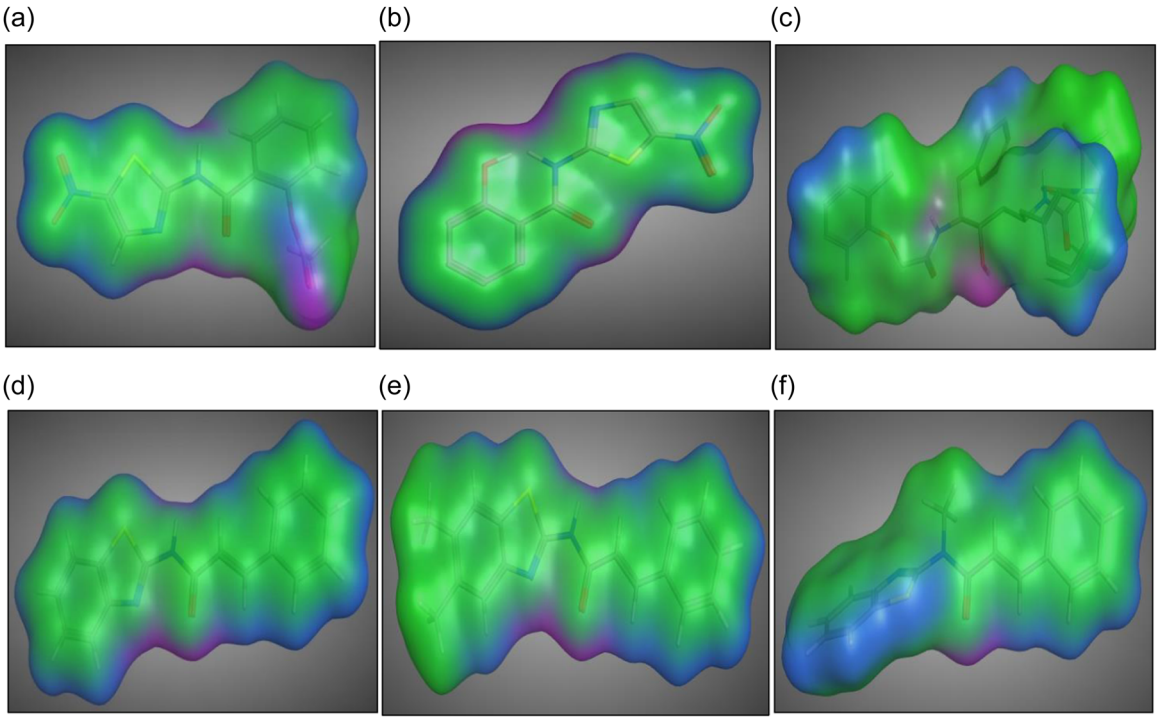

FIGURE 7 Active lone pair surface mapping for (a) nitazoxanide, (b) tizoxanide, (c) lopinavir and the most promising compounds (d) **19**, (e) **20**, and (f) **21**. Pink: hydrophilic (H-bonding), blue: mild polar, green: hydrophobic.

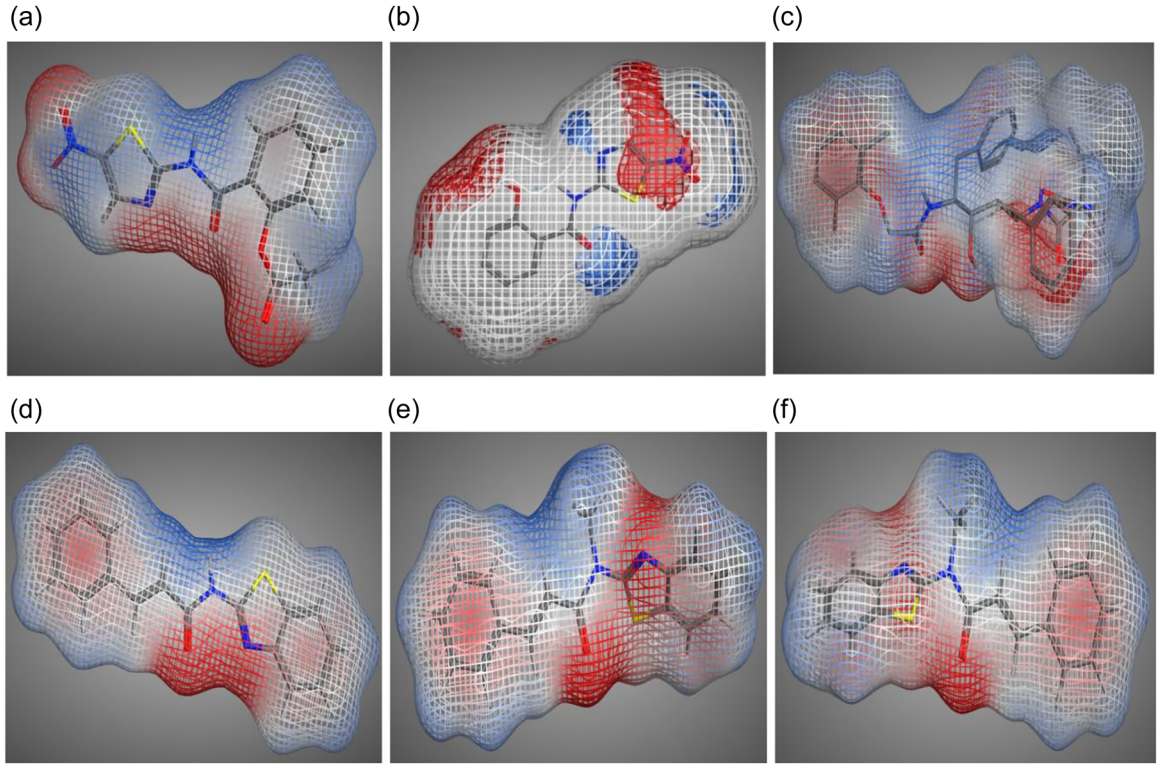

FIGURE 8 Electrostatics surface mapping for (a) nitazoxanide, (b) tizoxanide, (c) lopinavir and the most promising designed compounds (d) **19**, (e) **20**, and (f) **21**. Red: negative charge, white: neutral (zero charge), blue: positive charge.

orally active in human beings. These criteria are that molecular weight must not be more than 500 Da, log *p* (octanol–water partition coefficient) must not be more than five, hydrogen bond donors must not be more than five, hydrogen bond acceptors must not be more than 10, and the number of rotatable bonds must not be more than 10. In addition, this rule was further improved and stated that the compound with a total polar surface area of not more than 140 $Å^2$ would have good oral bioavailability.[25] As a part of the molecular modeling study, the compliance of the most promising designed compounds **19**, **20**, and **21** to Lipinski's rule of five was calculated using the Swiss ADME online website (http://www.swissadme.ch) and compared to nitazoxanide and lopinavir as illustrated in Table S2. From the obtained data, it can be observed that all of the promising designed compounds **19**, **20**, and **21** obey Lipinski's rule of five as well as the reference drugs, nitazoxanide, and lopinavir.

2.5 | In silico ADMET study

To reduce the risk of drug failure in the late phases of clinical trials, early absorption, distribution, metabolism, excretion, and toxicity (ADMET) properties prediction, and lead optimization must be done for earlier correction of pharmacokinetics ADMET property limitations.[26,27] For this reason, the blood–brain barrier (BBB) penetration, human intestinal absorption (HIA), aqueous solubility (log *S*), cytochrome P450 2D6 binding (one of the essential enzymes for drug metabolism), Ames toxicity, carcinogenicity and LD_{50} in a rat model were calculated using absorption, distribution, metabolism, excretion, and toxicity-structure activity relationship (ADMET-SAR)[28] for the most active compounds **19**, **20**, and **21**. ADMET data were calculated and collected in Table S3. Based on the predicted values of the ADMET data of nitazoxanide, lopinavir, and the tested compounds **19**, **20**, and **21**, the new compounds have comparable ADMET data with that of nitazoxanide and lopinavir (as reference drugs). The predicted ADMET data showed that the tested compounds are capable of penetrating BBB and can be absorbed by the human intestine. Their estimated log *S* values are very close to that of reference drugs. All of them are expected as nonsubstrate/noninhibitors of CYP-2D6 enzyme which suggests a low possibility of drug–drug interaction occurrence upon their administration. Furthermore, toxicity test data showed that all of these compounds are nontoxic nor-mutagenic in the Ames test and all are non-carcinogenic. The compounds LD_{50} doses in the rat model are comparable with that of nitazoxanide and lopinavir.

3 | CONCLUSION

The present study showed that compounds **19**, **20**, and **21** (Figure 9) could be considered active compounds for the treatment of COVID-19, having remarkable binding scores with the viral main protease, similar binding mode with additional new binding interactions attributed to new structural features, close surface mapping, and acceptable Lipinski's rule of five and ADMET data comparable to the reference drugs, nitazoxanide, and lopinavir. These compounds could be considered as a template for future investigation and development of SARS-CoV-2 viral protease inhibitors to help in fighting the coronavirus pandemic.

4 | EXPERIMENTAL

4.1 | Chemistry

4.1.1 | General remarks

Starting materials and reagents were purchased from Sigma-Aldrich Co., El-Gomhoria, and El-Nasr Pharmaceutical and Chemical Co. Reaction times were monitored using thin-layer chromatography on silica gel plates 60F245 E. Merck, using chloroform alone chloroform/methanol 9.9:0.1 as an eluting system and the spots were visualized by UV (366–245 nm). Stuart melting point apparatus SMP30 was used to measure melting points for all synthesized compounds. Bruker Avance III HD FT-high resolution ^1H nuclear magnetic resonance (NMR) (400 MHz), ^{13}C NMR (100 MHz) at Faculty of Pharmacy–Mansoura University was used to record ^1H, ^{13}C NMR spectra; chemical shifts are expressed in δ (ppm) with reference to TMS. A mass analyzer in Thermo Scientific GCMS model ISQ at the Regional Center for Mycology and Biotechnology (RCMB), Al-Azhar University, Nasr City, Cairo was used to record mass spectra. Elemental analyses were determined at the RCMB, Al-Azhar University, Nasr City, Cairo; and results were within ±0.4% of the calculated values for the suggested formulae. COV-3CL protease assay was performed at the confirmatory diagnostic unit, VACSERA. Compound *N*-(benzo[*d*]thiazol-2-yl)cinnamamide (**19**) was previously reported.[29] All other synthesized compounds are new ones.

The NMR spectra of the investigated compounds are provided in the Supporting Information. The InChI codes of the investigated

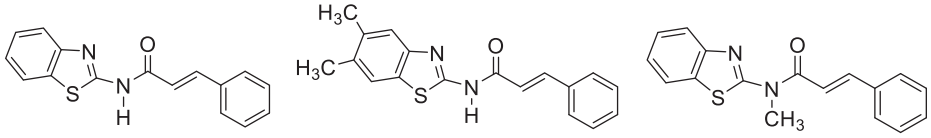

19: 22.61 ± 1.20 μM **20:** 14.70 ± 0.78 μM **21:** 21.99 ± 1.16 μM

FIGURE 9 Structures of the most active compounds **19**, **20**, and **21** as SARS-CoV-2 protease (COV M^{pro}) inhibitors. SARS-CoV-2, severe acute respiratory syndrome coronavirus 2.

compounds, together with some biological activity data, are also provided as Supporting Information.

4.1.2 | General procedure for the synthesis of 4- or 5-substituted *N*-(thiazol-2-yl)cinnamamides (**5–7**, **13**, **14**, **20**)

A solution of 4- or 5-substituted-thiazol-2-amine (**1–3**, **11**, **12**, **17**, **18**; 0.002 mol) and cinnamoyl chloride (**4**; 0.5 g, 0.003 mol) in pyridine (5 ml) was stirred for 12 h at room temperature, then the reaction mixture was poured into ice, filtered, washed with water and dried. The resulted residue was recrystallized from ethanol to give (**5–7**, **13–14**, and **20**).

N-*(5-Bromo-thiazol-2-yl)cinnamamide (**5**)*

Buff crystals (72%.), m.p. 238-243°C. ^{1}H-NMR ($CDCl_3$): δ 6.64 (d, 1H, J = 15.7 Hz, olefinic CH), 7.44 (s, 1H, ArH), 7.45–7.47 (m, 3H, ArH), 7.59, 7.62 (m, 2H, ArH), 7.91 (d, 1H, J = 15.7 Hz, olefinic CH). ^{13}C-NMR: δ 117.0 (allylic), 128.4 (aromatic), 128.6 (aromatic), 128.9 (aromatic), 129.1 (aromatic), 129.2 (aromatic), 131.3 (aromatic), 133.7 (allylic), 163.7 (aromatic), 164.0 (carbonyl). MS (*m*/*z*, %) for $C_{12}H_9BrN_2OS$: (M+2 310.3, 9), 131 (100).

N-*(5-Methyl-thiazol-2-yl)cinnamamide (**6**)*

White crystals (75%), m.p. 220-221°C. ^{1}H-NMR ($CDCl_3$): δ 2.47 (s, 3H, CH_3), 6.75 (d, 1H, J = 15.7 Hz, olefinic CH), 7.20 (s, 1H, ArH), 7.44–7.45 (m, 3H, ArH), 7.58–7.60 (m, 2H, ArH), 7.89 (d, 1H, J = 15.7 Hz, olefinic CH). ^{13}C-NMR: δ 11.8 (methyl), 118.7 (allylic), 128.1 (aromatic), 128.2 (aromatic), 129.0 (aromatic), 130.5 (aromatic), 132.5 (aromatic), 134.4 (aromatic), 144.2 (allylic), 158.9 (aromatic), 163.6 (carbonyl). MS (*m*/*z*, %) for $C_{13}H_{12}N_2OS$: (M+2 246.1, 25), (M +1 244.9, 72), 160 (100).

*Ethyl 2-cinnamamido-thiazole-4-carboxylate (**7**)*

White crystals (83%.), m.p. 215-223°C. ^{1}H-NMR ($CDCl_3$): δ 1.37 (t, 3H, J = 6.9 Hz, CH_3), 2.75 (s, 1H, NH), 4.37 (quartet, 2H, J = 6.9 Hz, CH_2), 6.76 (d, 1H, J = 15.6 Hz, olefinic CH), 7.40–7.41 (m, 3H, ArH), 7.56, 7.57 (m, 2H, ArH), 7.89 (d, 1H, J = 15.6 Hz, olefinic CH), 7.92 (s, 1H, ArH). ^{13}C-NMR: δ 14.3 (methyl), 61.8 (methelene), 118.3 (allylic), 122.5 (aromatic), 128.4 (aromatic), 129.0 (aromatic), 130.8 (aromatic), 134.1 (aromatic), 140.1 (aromatic), 145.1 (allylic), 160.0 (aromatic), 160.9 (carbonyl), 164.4 (carbonyl). MS (*m*/*z*, %) for $C_{15}H_{14}N_2O_3S$: (M^+ 302.5, 24), 66 (100).

N-*[4-(4-Bromo-phenyl)thiazol-2-yl]cinnamamide (**13**)*

Off white crystals (73%), m.p. 224-232°C. ^{1}H-NMR ($CDCl_3$): δ 6.29 (d, 1H, J = 16.0 Hz, olefinic CH), 7.25, 7.27 (m, 2H, ArH), 7.29 (s, 1H, ArH), 7.34–7.41 (m, 3H, ArH), 7.50 (d, 2H, J = 8, ArH), 7.75 (d, 2H, J = 8, ArH), 7.78 (d, 1H, J = 16.0 Hz, olefinic CH). ^{13}C-NMR: δ 108.6 (aromatic), 118.0 (allylic), 122.8 (aromatic), 127.7 (aromatic), 128.3 (aromatic), 128.9 (aromatic), 130.8 (aromatic), 132.0 (aromatic), 132.2 (aromatic), 134.0 (aromatic), 145.3 (allylic), 147.5 (aromatic), 160.1 (aromatic), 163.7 (carbonyl). MS (*m*/*z*, %) for $C_{18}H_{13}BrN_2OS$: (M+2 386.1, 48), (M^+ 384.2, 37), 131 (100).

N-*[4-(p-Tolyl)thiazol-2-yl]cinnamamide (**14**)*

Greenish white crystals (83%), m.p. 156-162°C. ^{1}H-NMR ($CDCl_3$): δ 2.31 (s, 3H, CH_3), 6.38 (d, 1H, J = 15.7 Hz, olefinic CH), 7.19 (s, 1H, ArH), 7.24 (d, 2H, J = 7.9 Hz, ArH), 7.29–7.41 (m, 5H, ArH), 7.77 (d, 2H, J = 7.9 Hz, ArH), 7.82 (d, 1H, J = 15.7 Hz, olefinic CH). ^{13}C-NMR: δ 21.2 (methyl), 107.1 (aromatic), 118.1 (allylic), 126.1 (aromatic), 128.4 (aromatic), 128.8 (aromatic), 129.8 (aromatic), 130.6 (aromatic), 134.0 (aromatic), 139.2 (aromatic), 145.2 (allylic), 147.6 (aromatic), 160.6 (aromatic), 163.8 (carbonyl). MS (*m*/*z*, %) for $C_{19}H_{16}N_2OS$: (M+2 322.3, 8), (M+1 321.4, 23), (M^+ 320.4, 100).

N-*(5,6-Dimethylbenzo[d]thiazol-2-yl)cinnamamide (**20**)*

Off white crystals (71%), m.p. 206-213°C. ^{1}H-NMR ($CDCl_3$): δ 2.29 (s, 3H, CH_3), 2.43 (s, 3H, CH_3), 6.73 (d, 1H, J =15.6 Hz, olefinic CH), 7.33, 7.42 (m, 3H, ArH), 7.45–7.47 (m, 2H, ArH), 7.63 (s, 1H, ArH), 7.68 (s, 1H, ArH), 7.93 (d, 1H, J = 15.6 Hz, olefinic CH). ^{13}C-NMR: δ 20.2 (methyl), 20.3 (methyl), 117.7 (allylic), 118.3 (aromatic), 122.1 (aromatic), 128.3 (aromatic), 128.7 (aromatic), 128.7 (aromatic), 129.0 (aromatic), 129.1 (aromatic), 131.2 (aromatic), 133.8 (aromatic), 143.0 (allylic), 145.6 (aromatic), 164.1 (carbonyl), 174.5 (aromatic). MS (*m*/*z*, %) for $C_{18}H_{16}N_2OS$: (M+2 310.0, 11), (M^+ 308.4, 22), 89 (100).

4.1.3 | General procedure for the synthesis of 4- or 5-substituted *N*-methyl-*N*-(thiazol-2-yl)cinnamamides (**8–10**, **15**, **16**, **21**, **22**)

A solution of 4- or 5-substituted *N*-(thiazol-2-yl)cinnamamide (**5–7**, **13**, **14**, **19**, **20**; 0.001 mol), methyl iodide (2 ml), and potassium carbonate anhydrous (0.2 g) in $CHCl_3$ (25 ml) was stirred at 40°C for 6 h. Then, the reaction mixture was filtered to remove excess potassium carbonate, washed with $CHCl_3$, the filtrate was evaporated using rotavap, and the resulted residue was boiled with hexane, filtered, and dried to obtain **8–10**, **15**, **16**, **21**, **22**.

N-*(5-Bromo-thiazol-2-yl)*-N-*methyl-cinnamamide (**8**)*

Light brown crystals (75%), m.p. 197-202°C, ^{1}H-NMR ($CDCl_3$): δ 3.86 (s, 3H, CH_3), 6.97 (d, 1H, J = 15.8 Hz, olefinic CH), 7.03 (s, 1H, ArH), 7.38–7.43 (m, 3H, ArH), 7.61–7.63 (m, 2H, ArH), 7.85 (d, 1H, J = 15.8 Hz, olefinic CH)). ^{13}C-NMR: δ 36.3 (methyl), 99.6 (aromatic), 125.0 (allylic), 127.0 (aromatic), 128.1 (aromatic), 128.8 (aromatic), 129.7 (aromatic), 135.4 (aromatic), 142.6 (allylic), 166.9 (carbonyl), 173.9 (aromatic). MS (*m*/*z*, %) for $C_{13}H_{11}BrN_2OS$: (M+2 325.5, 21.8), (M^+ 323.7, 25.9), 146 (100).

N-*Methyl*-N-*(5-methyl-thiazol-2-yl)cinnamamide (**9**)*

Off white crystals (79%), m.p. 153-156°C. ^{1}H-NMR ($CDCl_3$): δ 2.36 (s, 3H, CH_3), 3.94 (s, 3H, CH_3), 6.76 (s, 1H, ArH), 7.19 (d, 1H, J = 15.8 Hz, olefinic CH), 7.37–7.44 (m, 3H, ArH), 7.63–7.65 (m, 2H, ArH), 7.85 (d,

1H, J = 15.8 Hz, olefinic CH)). ^{13}C-NMR: δ 12.5 (methyl), 36.9 (methyl), 123.8 (allylic), 124.2 (aromatic), 128.3 (aromatic), 128.8 (aromatic), 129.8 (aromatic), 130.9 (aromatic), 135.4 (aromatic), 142.9 (allylic), 165.2 (aromatic), 171.8 (carbonyl). MS (*m*/*z*, %) for $C_{14}H_{14}N_2OS$: (M+1 259.4, 14), 51 (100).

*Ethyl 2-(*N*-methyl-cinnamamido)thiazole-4-carboxylate* (**10**)
Off white crystals (76%), m.p. 155-158°C. ^{1}H-NMR ($CDCl_3$): δ 1.43 (t, 3H, J = 7.04 Hz, CH_3), 4.00 (s, 3H, CH_3), 4.42 (quartet, 2H, J = 7.04 Hz, CH_2), 7.12 (d, 1H, J = 15.4 Hz, olefinic CH), 7.39–7.46 (m, 3H, ArH), 7.62–7.64 (m, 2H, ArH), 7.91 (s, 1H, ArH), 7.97 (d, 1H, J = 15.4 Hz, olefinic CH). ^{13}C-NMR: δ 14.4 (methyl), 35.4 (methyl), 61.3 (methylene), 115.6 (allylic), 124.0 (aromatic), 128.4 (aromatic), 128.6 (aromatic), 128.9 (aromatic), 129.1 (aromatic), 130.8 (aromatic), 134.4 (aromatic), 146.7 (allylic), 161.9 (carbonyl), 166.1 (carbonyl). MS (*m*/*z*, %) for $C_{16}H_{16}N_2O_3S$: (M+2 318.3, 10), (M+1 317.4, 37), (M^+ 316.3, 100).

N-*[4-(4-Bromo-phenyl)thiazol-2-yl]*-N-*methyl-cinnamamide* (**15**)
Yellowish crystals (78%), m.p. 130-136°C. ^{1}H-NMR ($CDCl_3$): δ 4.02 (s, 3H, CH_3), 7.14 (d, 1H, J = 15.5 Hz, olefinic CH), 7.26 (s, 1H, ArH), 7.46–7.47 (m, 3H, ArH), 7.56 (d, 2H, J = 8.2 Hz, ArH), 7.64–7.65 (m, 2H, ArH), 7.82 (d, 2H, J = 8.2 Hz, ArH), 7.98 (d, 1H, J = 15.5 Hz, olefinic CH). ^{13}C-NMR: δ 33.7 (methyl), 109.9 (aromatic), 116.1 (allylic), 127.6 (aromatic), 128.3 (aromatic), 128.4 (aromatic), 129.0 (aromatic), 129.1 (aromatic), 129.6 (aromatic), 130.7 (aromatic), 131.5 (aromatic), 131.8 (aromatic), 146.3 (allylic), 157.8 (aromatic), 165.8 (carbonyl). MS (*m*/*z*, %) for $C_{19}H_{15}BrN_2OS$: (M+2 401.4, 10), (M^+ 399.0, 12), 270 (100).

N-*Methyl*-N-*[4-(*p*-tolyl)thiazol-2-yl]cinnamamide* (**16**)
Greenish white crystals (87%), m.p. 175-182°C. ^{1}H-NMR ($CDCl_3$): δ 2.41 (s, 3H, CH_3), 3.93 (s, 3H, CH_3), 7.15 (d, 1H, J = 15.4 Hz, olefinic CH), 7.19 (s, 1H-Ar-H), 7.25 (d, 2H, J = 7.9 Hz, ArH), 7.45–7.46 (m, 3H, ArH), 7.63–7.65 (m, 2H, ArH), 7.84 (d, 2H, J = 7.9 Hz, ArH), 7.97 (d, 1H, J = 15.4 Hz, olefinic CH). ^{13}C-NMR: δ 21.3 (methyl), 35.6 (methyl), 108.8 (aromatic), 116.2 (allylic), 126.0 (aromatic), 127.9 (aromatic), 128.3 (aromatic), 129.0 (aromatic), 129.4 (aromatic), 130.6 (aromatic), 134.7 (aromatic), 137.7 (aromatic), 146.0 (allylic), 146.7 (aromatic), 149.5 (aromatic), 165.6 (carbonyl). MS (*m*/*z*, %) for $C_{20}H_{18}N_2OS$: (M+2 336.3, 12), (M+1 335.4, 36), (M^+ 334.5, 100).

N-*(Benzo[d]thiazol-2-yl)*-N-*methyl-cinnamamide* (**21**)
Buff crystals (81%), m.p. 170-176°C. ^{1}H-NMR ($CDCl_3$): δ 3.98 (s, 3H, CH_3), 6.93 (d, 1H, J = 15.9 Hz, olefinic CH), 7.33–7.44 (m, 5H, ArH), 7.48–7.52 (m, 1H, ArH), 7.63–7.65 (m, 2H, ArH), 7.69–7.76 (m, 1H, ArH), 7.93 (d, 1H, J = 15.9 Hz, olefinic CH). ^{13}C-NMR: δ 32.3 (methyl), 111.2 (aromatic), 122.9 (allylic), 123.9 (aromatic), 126.2 (aromatic), 126.9 (aromatic), 127.0 (aromatic), 128.1 (aromatic), 128.8 (aromatic), 129.6 (aromatic), 135.5 (aromatic), 137.3 (aromatic), 142.4 (allylic), 167.3 (carbonyl), 175.3 (aromatic). MS (*m*/*z*, %) for $C_{17}H_{14}N_2OS$: (M+2 296.6, 29), (M+1 294.9, 44), 66 (100).

N-*(5,6-Dimethyl-benzo[d]thiazol-2-yl)*-N-*methyl-cinnamamide* (**22**)
Buff crystals (83%), m.p. 236-239°C. ^{1}H-NMR ($CDCl_3$): δ 2.38 (s, 3H, CH_3), 2.43 (s, 3H, CH_3), 4.00 (s, 3H, CH_3), 7.01 (d, 1H, J = 15.7 Hz, olefinic CH), 7.19 (s, 1H, ArH), 7.40–7.42 (m, 3H, ArH), 7.49 (s, 1H, ArH), 7.64–7.65 (m, 2H, ArH), 7.91 (d, 1H, J = 15.7 Hz, olefinic CH). ^{13}C-NMR: δ 19.8 (methyl), 20.5 (methyl), 33.0 (methyl), 112.5 (aromatic), 120.1 (allylic), 123.1 (aromatic), 124.0 (aromatic), 126.4 (aromatic), 128.3 (aromatic), 128.5 (aromatic), 128.8 (aromatic), 129.9 (aromatic), 135.5 (aromatic), 145.4 (allylic), 148.8 (aromatic), 163.2 (aromatic), 166.5 (carbonyl). MS (*m*/*z*, %) for $C_{19}H_{18}N_2OS$: (M+2 324.2, 27), (M^+ 322.1, 100).

4.2 | COV2-3CL protease inhibition assay

The COV2-3CL protease enzyme assay[15,16] was performed by adding 30 µl of 3CL protease and 10 µl of compound diluted in 1× assay buffer. Then Incubated for 30 min at room temperature. The reaction started by adding 10 µl of the diluted substrate. Then Incubated at room temperature overnight and the plate was sealed with the plate sealer. The fluorescence intensity was measured in a microtiter plate-reading fluorimeter capable of excitation at a wavelength of 360 nm and detection of emission at a wavelength of 460 nm. The fluorescence intensity can also be measured kinetically. The "Blank" value is subtracted from all other values. Results are reported as % inhibition of enzymatic activity (Table 1).

4.3 | Molecular modeling study

The binding affinity of the designed compounds **5–10**, **13–16**, **and 19–22** to the SARS-CoV-2 main protease binding pocket amino acids residues was predicted by carrying out a docking experiment and comparing their results to nitazoxanide as a reference drug. The structures of the proposed newly synthesized compounds were built using the builder tool of MOE version 2009.11 (Chemical Computing Group Inc. software (https://www.chemcomp.com/)).[30] Preparation of the ligands was performed by minimizing their energy to get their most stable conformers that are ready for docking into the SARS-CoV-2 main protease (COV Mpro) active site. Structures of the ligands were minimized by adopting the Molecular Mechanics Force Field (MMFF94x) forcefield until an RMSD gradient of 0.05 kcal/mol/Å was reached. For each ligand, energy minimizations were performed using 1000 steps of steepest descent. The prepared ligands were docked into the binding site of SARS-CoV-2 main protease in complex with an inhibitor **N3** (PDB code ID: 6LU7)[11] and were used as the target enzyme. Target enzyme preparation for the docking process was performed by adding the hydrogen atoms, then the target structure was refined by adding the missed atoms and bonds, followed by fixing the target potential. The active site was defined as the region of Covid-19 main protease that comes within 10 Å from the ligand.[31] Conformational analysis of the compounds was performed using MMFF94 force-field[20] (with RMS gradient of

0.01 kcal/Å mol) implemented in MOE 2009.10.13. The flexible alignment was done using MOE/MMFF94 flexible alignment tool.[32] Two-hundred conformers of each compound were generated and minimized with a distance-dependent dielectric model. A set of 100 conformers having the least energy was selected for further analysis. Then, the alignment with the lowest strain energy and highest alignment scoring was selected and shown in the study. Surface mapping figures were done using MOE software. In the active LP surface maps, the pink-colored regions showed high hydrogen-bonding ability, blue-colored regions are mild polar, and green colored ones are the lipophilic regions, while in the electrostatics surface maps, the red-colored regions indicate negatively charged sites, the white-colored regions indicate neutral sites with zero charge and the blue colored regions indicate positively charged sites.

ACKNOWLEDGMENTS

The authors would like to express our sincere gratitude to the NMR Unit at the Faculty of Pharmacy-Mansoura University Bruker Avance III HD FT-high resolution—^{1}H NMR (400 MHz), ^{13}C NMR (100 MHz) for support.

CONFLICT OF INTEREST

The authors declare no conflict of interest.

ORCID

Selwan M. El-Sayed http://orcid.org/0000-0003-3962-6409

REFERENCES

[1] X. Yang, Y. Yu, J. Xu, H. Shu, H. Liu, Y. Wu, L. Zhang, Z. Yu, M. Fang, T. Yu, Y. Wang, *Lancet Respir. Med.* **2020**, *8*(5), 475.
[2] K. Kupferschmidt, J. Cohen, *Science* **2020**, *367*(6478), 610.
[3] G. Li, E. De. Clercq, *Nat. Rev. Drug Discov.* **2020**, *19*, 149.
[4] N. H. El-Subbagh, R. Rabie, A. A. Mahfouz, K. M. Aboelsuod, M. Y. Elshabrawy, H. M. Abdelaleem, B. E. Elhammady, W. Abosaleh, L. A. Salama, S. Badreldeen, M. Yasser, *J. Disaster Res.* **2021**, *16*(1), 70.
[5] E. Dong, H. Du, L. Gardner, *Lancet Infect. Dis.* **2020**, *20*(5), 533.
[6] S. J. Anthony, C. K. Johnson, D. J. Greig, S. Kramer, X. Che, H. Wells, A. L. Hicks, D. O. Joly, N. D. Wolfe, P. Daszak, W. Karesh, *Virus Evol.* **2017**, *3*(1), vex012.
[7] A. Hegyi, J. Ziebuhr, *J. Gen. Virol.* **2002**, *83*(3), 595.
[8] C. Liu, Q. Zhou, Y. Li, L. V. Garner, S. P. Watkins, L. J. Carter, J. Smoot, A. C. Gregg, A. D. Daniels, S. Jervey, D. Albaiu, *Am. Chem. Soc.* **2020**, *6*(3), 315.
[9] K. Anand, J. Ziebuhr, P. Wadhwani, J. R. Mesters, R. Hilgenfeld, *Science* **2003**, *300*(5626), 1763.
[10] D. Needle, G. T. Lountos, D. S. Waugh, *Acta Crystallogr., Sect. D: Biol. Crystallogr.* **2015**, *71*(5), 1102.
[11] Z. Jin, X. Du, Y. Xu, Y. Deng, M. Liu, Y. Zhao, B. Zhang, X. Li, L. Zhang, C. Peng, *Nature* **2020**, *582*(7811), 289.
[12] D. B. Mahmoud, Z. Shitu, A. Mostafa, *J. Genet. Eng. Biotechnol.* **2020**, *18*(1), 1.
[13] Y. I. El-Gazzar, H. H. Georgey, S. M. El-Messery, H. A. Ewida, G. S. Hassan, M. M. Raafat, M. A. Ewida, H. I. El-Subbagh, *Bioorg. Chem.* **2017**, *72*, 282.
[14] H. I. El-Subbagh, G. S. Hassan, A. S. El-Azab, A.A.-M. Abdel-Aziz, A. A. Kadi, A. M. Al-Obaid, O. A. Al-Shabanah, M. M. Sayed-Ahmed, *Eur. J. Med. Chem.* **2011**, *46*, 5567.
[15] J. S. Morse, T. lalonde, S. Xu, W. R. Liu, *ChemBioChem* **2020**, *21*(5), 730.
[16] L. Zhang, D. Lin, X. Sun, U. Curth, C. Drosten, L. Sauerhering, S. Becker, K. Rox, R. Hilgenfeld, *Science* **2020**, *368*(6489), 409.
[17] A. Saxena, D. Wong, K. Diraviyam, D. Sept, *Methods Enzymol.* **2009**, *467*, 307.
[18] L. G. Ferreira, N. Ricardo Dos Santos, O. Glaucius, D. Adriano, *Molecules* **2015**, *20*, 13384.
[19] W. Tachoua, M. Kabrine, M. Mushtaq, Z. Ul-Haq, *J. Mol. Graphics Modell.* **2020**, *101*, 107758.
[20] T. A. Halgren, *J. Comput. Chem.* **1996**, *17*(5-6), 520.
[21] P. Labute, C. Williams, M. Feher, E. Sourial, J. M. Schmidt, *J. Med. Chem.* **2001**, *44*(10), 1483.
[22] K. W. Lexa, H. A. Carlson, *Q. Rev. Biophys.* **2012**, *45*(3), 301.
[23] L. T. Lin, W. C. Hsu, C. C. Lin, *J. Tradit. Complement. Med.* **2014**, *4*(1), 24.
[24] D. E. Clark, S. D. Pickett, *Drug Discov. Today* **2000**, *5*(2), 49.
[25] W. P. Walters, *Expert Opin. Drug Discov.* **2012**, *7*(2), 99.
[26] M. T. H. Khan, *Curr. Drug Metab.* **2010**, *11*(4), 285.
[27] M. S. Shanker, *J. Chem. Inf. Comput. Sci.* **1996**, *36*(1), 35.
[28] H. Yang, C. Lou, L. Sun, J. Li, Y. Cai, Z. Wang, W. Li, G. Liu, Y. Tang, *Bioinformatics* **2019**, *35*(6), 1067.
[29] S. Premaletha, A. Ghosh, S. Joseph, S. R. Yetra, A. T. Biju, *Chem. Commun.* **2017**, *53*(9), 1478.
[30] MOE. 10 of Chemical Computing Group. Inc. **2009**. https://www.chemcomp.com/ (accessed: May 15, 2022).
[31] A. E. Allam, H. K. Assaf, H. A. Hassan, K. Shimizu, Y. A. Elshaier, *RSC Adv.* **2020**, *10*(50), 29983.
[32] Y. Inbar, D. Schneidman-Duhovny, O. Dror, R. Nussinov, H. J. Wolfson**2007**, preseneted at Annu. Int. Conf. Res. Comput. Mol. Biol., **2007**. pp. 412-429.

SUPPORTING INFORMATION

Additional supporting information can be found online in the Supporting Information section at the end of this article.

How to cite this article: R. W. Elsayed, M. A. Sabry, H. I. El-Subbagh, S. M. Bayoumi, S. M. El-Sayed, *Arch. Pharm.* **2022**;355:e2200121. https://doi.org/10.1002/ardp.202200121